Available online at www.garmian.edu.krd

Passer Journal

Passer 5 (Issue 2) (2023) 278-289

http://passer.garmian.edu.krd/

Synthesis of $CoFe_2O_4/SiO_2$ nanoparticles and investigation of their magnetic, dielectric, and structural characteristics

Jwan Saeed Jumaa[1,3]*, Salah Raza Saeed[2], Ali Mustafa Mohammad[3]

[1]*Department of Physics, College of Science, Charmo University, Chamchamal, Kurdistan Region, Iraq.*
[2]*Department of Physics, College of Science, University of Sulaimani, Sulaimani, Kurdistan Region, Iraq.*
[3]*Department of Physics, College of Education, University of Garmian, Garmian, Kurdistan Region, Iraq.*

Received 02 April 2023; revised 21 May 2023;
accepted 21 May 2023; available online 07 June 2023

DOI: 10.24271/PSR.2023.391586.1302

ABSTRACT

Using the sol-gel auto-combustion method, $CoFe_2O_4/SiO_2$ ferrite nanocomposites (SiO_2=0, 20, 40, and 60%) were synthesized. The impact of temperature on a material's structural, magnetic, and electrical characteristics was investigated in this study. Infrared spectroscopy and X-ray diffraction revealed that ferrite crystalizes in the cubic spinel phase, as demonstrated by the use of patterns. Ferrite crystallite size ranges from 33.36 and 46.50 nm (depending on calcination) and 43.89 and 49.05 nm (depending on SiO_2 mixing ratio). FE-SEM demonstrates that calcination temperature affects the particle size, as does the amount of SiO_2 in the mixture. The EDS was utilized to confirm that each sample contained all of the required elements. VSM measurements were performed on all pure and doped samples that exhibited ferromagnetic behavior at various calcination temperatures and SiO_2 mixing ratios. At room temperature, the LCR meter was utilized to carry out an analysis of the electrical properties of each sample. Changes in dielectric characteristics have been observed at frequencies between 50 Hz and 1 MHz, following the theory of Koop's, Maxwell-Wagner polarization, and hopping of electrons. As the frequency was increased observable natural behavior was evident in all of the dielectric properties. In this study silica, coated ferrite (Co_{1-X} Mgx Fe_2O_4)/SiO_2 nanoparticles have been investigated to find out the impact of silica on magnetic and electrical properties.

Keywords: Nanocomposite; Spinel Ferrites; VSM; Sol-Gel Method; Dielectric Properties.

1. Introduction

The emergence of nanotechnology has expanded the scope of possibilities for material manipulation at the nanoscale, presenting new opportunities for human achievement. Since the turn of the century, nanoparticles have been regularly examined and utilized in several industrial applications[1, 2]. On account of their extraordinary biological, chemical, and physical properties, nanomaterials with unique chemical composition, size, and shape control have been used across many fields[3, 4]. Because of the high surface/interface modifications compared to bulk material, magnetic nanostructures have many remarkable electrical and magnetic properties and exceptional features at the nanometer range, such as mechanical hardness, coercivity, spin-glass behavior, and super para-magnetism, etc.[5]. Spinel ferrite specifically an AB_2O_4 type nanoparticle has a broad and scalable field that has attracted significant interest from many research groups in applied research. In recent years, the special chemical, physical, and biological properties of nanocrystalline shapes have considerable attention from academics, because of their potential application in various fields. These fields include magnetic recording, ferrofluids, biomedicine, spintronics, gas sensors, magnetic hyperthermia, and drug targeting[3, 6]. The mineral known as cobalt ferrite belongs to the spinel family and consists of chemicals that have the general formula $MeFe_2O_4$, where Me refers to metal (Zn, Co, Ni, etc.)[7]. $CoFe_2O_4$ is typically a semi-inversed ferrite in which the majority of cobalt ions are found to occupy B sites, whereas the distribution of Fe^{3+} ions is observed to be relatively uniform across the sites (A and B)[10]. $CoFe_2O_4$ material exhibits ferromagnetic behavior and possesses a high Curie temperature of approximately 793 K. Additionally, it displays strong magnetocrystalline-anisotropy and moderate magnetization (*Ms*), rendering it a hard magnetic material, and high coercivity (*Hc*)[8]. Because of these characteristics, cobalt ferrite is an excellent possibility in high-density digital recording disks and magnetic recording applications, etc...Various techniques have been developed for spinel ferrite nanostructures such as chemical co-precipitation[9], microemulsion[10], sol-gel[11], hydrothermal[12], ball milling[13], etc.

* Corresponding author
E-mail address: jwanasadsaeedjumaa@gmail.com (Instructor).
Peer-reviewed under the responsibility of the University of Garmian.

In a study done by S.R. Mekala and J. Ding[14], the addition of SiO_2 was investigated as a means of improving the magnetism and electrical properties of a composite material. The results indicated that the incorporation of a small quantity of 4.5 wt% silica was effective in conferring favorable magnetic characteristics to the composite, as evidenced by a coercivity of 3 kOe and a saturation magnetization of 72 emu/g. According to Somayyeh R. et al.[15], Silica-coated ferrite, $(CoFe_2O_4)/SiO_2$, can be utilized to improve the magnetic properties of nanoparticles and has potential biological applications. Chen, Ching-Cheng, Yen-Pei Fu, et al.[16] effectively prepare a TiO_2/SiO_2/Ni-Cu-Zn ferrite composite with high photocatalytic activity for magnetic photocatalysts. Based on the findings of research carried out by K. Nadeem et al.[17], the concentration of amorphous silica (SiO_2) matrix affects the electrical properties as well. Their investigation revealed that the small polaron hopping in these nanoparticles contributes to the increase in ac conductivity at higher frequencies.

The Sol-gel auto-combustion method was utilized in the synthesis process due to its ease of use, cheap cost, and high proportion of homogenous and acceptable nanoparticles[1]. In the first section of this investigation, the influence that changes in temperature have on the magnetic characteristics, as well as the structure and morphology of $CoFe_2O_4$ samples are examined. Elevating the calcination process temperature exerts a noteworthy influence on the structure of cobalt ferrite spinel, crystal size, particle size, and porosity, as well as the magnetic characteristics of cobalt ferrite. The second part is, after adding silica to $CoFe_2O_4$ samples, which calcined at 700 °C in ratios of 0%, 20%, 40%, and 60%, the above parameters were evaluated, and their electrical properties were studied.

2. Materials and Methods

2.1 Synthesis of CoFe2O4 and CoFe2O4/SiO2 nanocomposites

Nanoparticles of $CoFe_2O_4$ were prepared via a sol-gel auto-combustion route. To get a mixed solution, it is necessary to utilize stoichiometric amounts of citric acid $C_6H_8O_7$, ferric nitrate $Fe(NO_3)_3.9H_2O$, and cobalt nitrate $Co(NO_3)_2.6H_2O$, each sample was dissolved separately in the smallest possible amount of deionized water. The solutions that were acquired underwent a process of conversion into a gel phase with high viscosity. This was accomplished by gradually increasing the temperature of the heated plate to 90 °C for two hours while consistently stirring the mixture. Upon undergoing the evaporation process, the solution exhibited an increase in viscosity and eventually transformed into a dark gel with a highly viscous consistency. When the viscous gel was heated to 250 °C in an oven, the auto-combustion reaction yielded as-burned ferrite grains commenced. By milling a rough obtained powder in a mortar, the product was refined into a fine powder. The as-burned nanoferrite was calcined at several temperatures (500, 600, and 700 °C) to promote homogeneity and eliminate organic waste. This study endeavors to examine the influence of temperature on the structural, morphological, and magnetic characteristics of synthesized materials. $CoFe_2O_4/SiO_2$ samples were formed when $CoFe_2O_4$ samples calcined at 700 °C and doped with silica in ratios of (0%, 20%, 40%, and 60%), and were analyzed for their structural, morphological, and magnetic properties to comprehend the effect of silica dopant. To examine the electrical properties of $CoFe_2O_4$, samples calcined at 700 °C were combined with silica in the same proportion as described before, three drops of PVA were added as a binder, and after that, the mixture was compressed into pellets with a diameter of 13 millimeters and a thickness of 1-2 millimeters. This is achieved by applying a 2.5-ton for 1.5-minute hydraulic press pressure, and then sintering the samples for 3 hours at 800 °C to intensify them, and then allowing them to cool naturally so that the dielectric properties may very well be evaluated.

2.2 Characterizations

The PANalytical X'pert Pro diffractometer from the Netherlands has been used to obtain X-ray diffraction (XRD) patterns. The measured values spanned from 15° to 70°. The instrument utilized for diffraction analysis was outfitted with a high-intensity source of Cu kα radiation, with a wavelength of 0.154 nm. The morphology of the sample surface was analyzed using an FE-SEM (Model Mira3-XMU, TESCAN, Japan). The Fourier transform infrared spectroscopy was performed on all ferrite samples employing the Perkin Elmer FT-IR spectrometer, United States. KBr pellets were employed in the spectral range of 300 to 4000 cm^{-1}. The Vibrating Sample Magnetometer (VSM) was utilized to investigate the M-H hysteresis loops at room temperature. The applied fields were ±15 kOe, LBKFB model from Meghnatis Daghigh Kavir Company was used for the analysis. Dielectric measurements were acquired at room temperature using an LCR meter within the frequency range of 50Hz to 1MHz (KEYSIGHT E4980A).

3. Results and discussion

3.1 CoFe2O4 nanocomposites

3.1.1 XRD studies

The XRD patterns of cobalt ferrite $CoFe_2O_4$ are depicted in Figure 1. All of the diffraction peaks associated with cobalt ferrites (220), (311), (222), (400), (422), (511), and (440) are revealed in the XRD pattern. The peak positions within XRD patterns exactly correspond to the conventional pattern for pure $CoFe_2O_4$ with a code number ICSD 00-001-1121. According to the results, as the calcination temperature rises, all peaks grow together, causing the diffraction to reach its maximum and become sharper and narrower. This suggests that the augmentation of particle size in the nucleus leads to an increase in both the density of crystallization and the ratio of crystal size[18]. The results agree well with A. Mohammad, et al.[19]. Using the Scherrers formula the crystallite sizes (D) were estimated for each sample dependent on the full-width peak at half-maximum intensity (311)[20]:

$$D = \frac{0.9\,\lambda}{\beta \cos\theta} \quad (1)$$

The symbol λ represents the X-ray wavelength, while β denotes the full width at half maximum of the relevant peak. The calcination temperature exhibited a substantial effect on the crystallinity (Table 1). Variations in crystallite size were observed, ranging from 33.36 to 46.50 nm.

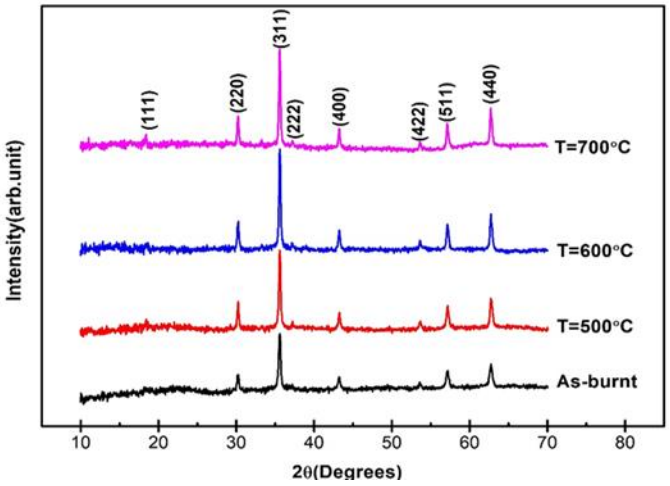

Figure 1: XRD patterns of CoFe2O4 nanoparticles at various temperatures.

Interplanar spacing was utilized to obtain the lattice parameter of $CoFe_2O_4$ nanoferrites using the following formula[21]:

$$a = d_{hkl}\sqrt{h^2 + k^2 + l^2} \quad (2)$$

The interplanar spacing, represented by *hkl*, is determined by the Miller indices of the lattice plane denoted by *h*, *k*, and *l*. Table 1 displays that the lattice parameter falls within a range of approximately 8.346 - 8.372 nm. The lattice value was seen growing as the temperature increased at 500 °C and subsequently started to decrease with elevated temperature. This behavior is identical to the previous report[22]. The equation utilized to find out the X-ray density ρ_x of the samples produced is as follows[9]:

$$\rho_x = \frac{8M}{Na^3} \quad (3)$$

where *N*, *M*, and 8 represent, respectively, the molecular weight, Avogadro's number, and the number of molecules per unit cell. The $\rho_x\ of$ cobalt ferrite ranged from 5.312 to 5.362 g/cm^3. It was found that the X-ray density increased in tandem with the calcination temperature, which meant that the higher the temperature, the denser the X-rays, this result is similar to previous studies[11].

The hopping length is the distance between magnetic ions located in the tetrahedral (A) and octahedral (B) sites, and it can be computed by using the calculations that are provided below[23]:

$$L_A = 0.25\ a\ \sqrt{3} \quad (4)$$

$$L_A = 0.25\ a\ \sqrt{2} \quad (5)$$

Notably, an alteration in the hopping length on both sides was observed with an increase in the calcination temperature (Table1).

Table 1: CoFe2O4 nanoferrites structural characteristics at various temperatures.

Composition	*Temp.* ℃	2 Theta	*FWHM*	*D* (nm)	*a*(Å)	ρ_x(g/cm^3)	L_A(Å)	L_B(Å)
$CoFe_2O_4$	as-burnt	35.576	0.2	41.70	8.363	5.328	3.621	2.957
	500	35.540	0.25	33.36	8.372	5.312	3.625	2.960
	600	35.554	0.19	43.90	8.368	5.319	3.623	2.958
	700	35.653	0.162	46.50	8.346	5.362	3.614	2.951

3.1.2 Fourier transform-infrared spectroscopy

FT-IR spectrum analysis identifies the location of ions in a crystal structure and supports spinel structure formation and cation distribution in nanocrystalline cobalt ferrite[24]. Figure 2 depicts the typical FT-IR spectra of ferrite samples at a temperature of 500, 600, and 700 °C. All spinel compounds below 1000 cm^{-1} conform to the two main absorption band vibrational modes v_1 and v_2 are visible in the spectra, which is a characteristic property of spinel ferrite[25]. The absorption bands observed in the study are assigned to the vibrational modes of the tetrahedral and octahedral metal complexes. Specifically, the higher frequency absorption band (v_1=572.86-574.79 cm^{-1}) corresponds to the vibration of the tetrahedral metal complex, which involves a linkage between the oxygen ion and the metal ion located at the tetrahedral site. The vibration of the octahedral metal complex, on the other hand, is attributed to the lower frequency absorption band (v_2=371.22-374.19 cm^{-1}), which entails a link between the oxygen ion and the metal ion at the octahedral site[12]. FT-IR analysis indicates an increase in calcination temperatures at various stages. Additionally, a consistent trend of peak displacement in the direction of higher frequencies for bands v_1 and lower frequencies for bands v_2 was observed indicating a mixed spinel state of $CoFe_2O_4$. The primary explanation for this behavior may be due to an alteration in the bond lengths that are formed between metal and oxygen ions at both tetrahedral and octahedral locations, which occurs as a result of a change in the calcination temperature[26].

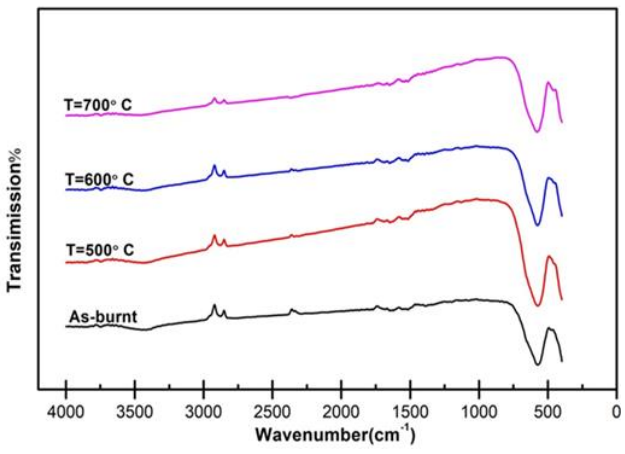

Figure 2: FT-IR spectra of CoFe2O4 nanoferrites at different temperatures.

Table 2: FT-IR spectroscopy wave number of CoFe2O4 nanoferrites at various temperatures.

Temp.˚C	*FT-IR frequency bands* (cm^{-1})	
	v_1	v_2
as-burnt	574.78	371.22
500	572.86	372.26
600	574.79	374.19
700	574.79	374.19

3.1.3 FE-SEM studies

Figure 3(a-d) depicts a typical FE-SEM image of nanoferrite samples at various calcination temperatures (as-burnt, 500, 600, and 700 °C). Some particles form enormous clusters as a consequence of the interaction between magnetic nanoparticles that occurs naturally. According to the FE-SEM, the grains in all of the samples were relatively well-crystallized. A large number of particles with a restricted grain size distribution were enumerated for precise measurements, and the average particle size and standard deviation for all samples were calculated. Table 3 displays the determined particle size of $CoFe_2O_4$ nanoparticles for as-burned and various calcined samples using two distinct methods, XRD and FE-SEM. The particle size determined by FE-SEM (using Image J software) is greater than that determined by XRD. This difference may be the consequence of the disorder in the molecular structure and the strain on the lattice that is created by the different radii of the ions and/or nanoparticle clustering[27].

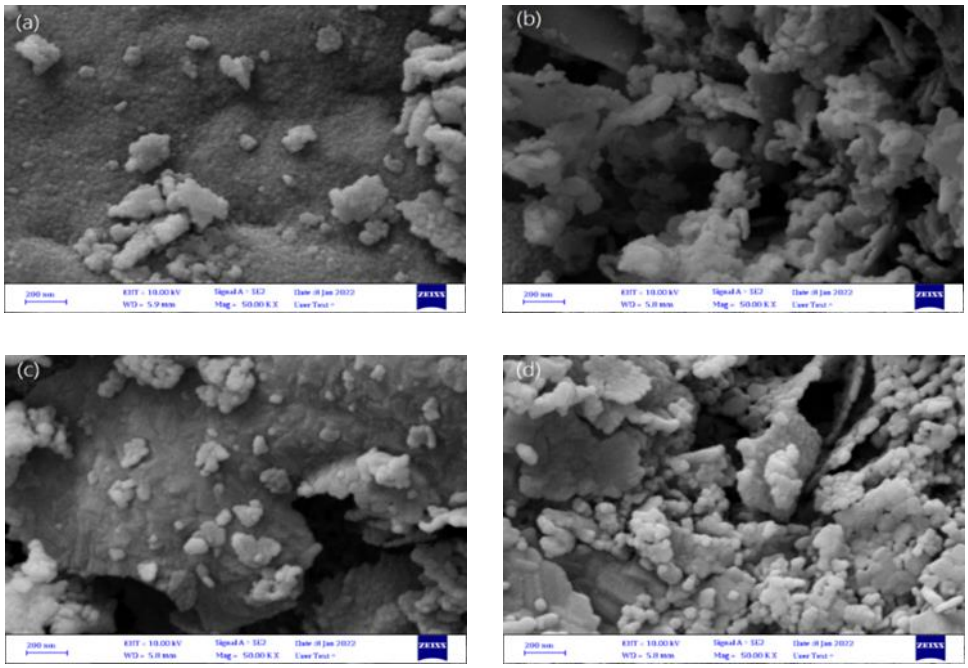

Figure 3: FE-SEM images of $CoFe_2O_4$ nanoferrites for (a) as-burnt (b) calcined samples at 500 ℃ (c) at 600 ℃ and (d) at 700 ˚C.

Table 3: Crystallite size and particle size of CoFe2O4 nanoferrites were estimated from XRD and FE-SEM respectively at various temperatures.

Composition	*Temp.*˚C	*D*(nm) XRD	*D*(nm) FE-SEM
$CoFe_2O_4$	As-burnt	41.70	42.02
	500	33.36	43.12
	600	43.90	45.34
	700	46.50	51.97

The EDS analysis was utilized to evaluate the chemical composition and weight ratios[24]. EDS examination reveals the production of the desired oxide metals, The observation suggests that the aforementioned metals have undergone chemical transformations. Hence, it is possible to ascertain both the chemical constitution and the weight proportions, as depicted in Figure 4. (a-d). The identified peaks indicate the presence of, Cobalt, iron, and Oxygen components, while no impurities were detected.

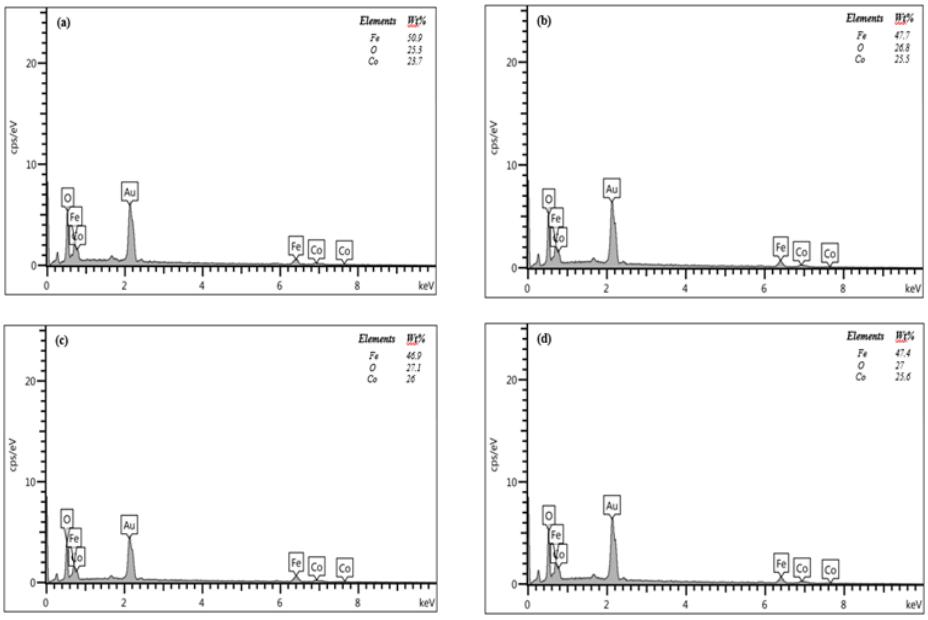

Figure 4: EDS spectra of $CoFe_2O_4$. nanoferrites for (a) as-burnt (b) calcined specimen at 500 ℃ (c) at 600 ℃ and (d) at 700 ℃.

3.1.4 Magnetic properties

Figure 5 depicts the magnetic hysteresis loops of all samples for $CoFe_2O_4$ nanoparticles synthesized at room temperature employing a VSM within an applied field range of ±15 kOe.

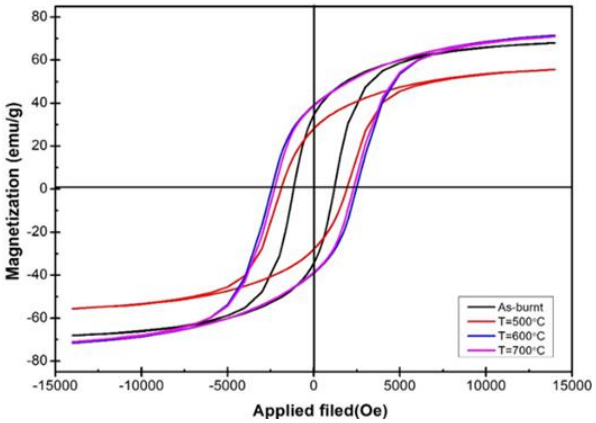

Figure 5: $CoFe_2O_4$ nanoferrites hysteresis curves for as-burned and various calcination temperatures.

The measured results of magnetic properties indicate that all of the samples exhibit ferrimagnetic properties. The coercivity (*Hc*) values, saturation magnetization values (*Ms*), and remanent magnetization (*Mr*) values of cobalt ferrite nanoparticles were determined through analysis of the hysteresis loops. The relationships for determining the theoretical magnetic moment (nB), squareness ratio (S), and magnetic anisotropy (K) are as follows, in order:[19].

$$nB = \frac{(M_{wt} * M_s)}{5585} \quad (6)$$

$$S = \frac{M_{wt}}{M_s} \quad (7)$$

$$H_C = \frac{(0.96*k)}{M_s} \quad (8)$$

where M_{wt} is the molecular weight.

The magnetic parameters derived from the hysteresis curves are displayed in Table 4. With a rise in calcination temperature, there is an observed elevation in both saturation (*Ms*) and remanence (*Mr*). It was observed that the saturation magnetization of cobalt ferrite nanoparticles varies with calcination temperature. Specifically, the highest saturation magnetization of 70.33469 emu.g^{-1} was recorded for particles calcined at 700 °C, while the lowest saturation magnetization of 55.58493 emu.g^{-1} was observed for particles calcined at 500 °C. The increase in saturation magnetization shift at the higher calcination temperature can be attributed to spin canting and surface spin disturbance in the nanoparticles[28]. A. Mohammad,et al.[27] also obtained similar observations.

Table 4: Magnetic properties of $CoFe_2O_4$ nanoferrites as affected by calcination temperature.

Composition	*Temp.*˚C	*Ms* (emu.g^{-1})	*Mr*(emu.g $^{-1}$)	*Hc*(Oe)	*nB* (μB)	*Mr/ Ms*	*K* × 10^3 (emu. Oeg^{-1})
$CoFe_2O_4$	As-burnt	66.600	34.383	1170.6	2.80	0.52	81.21
	500	55.585	29.1587	2000.3	2.33	0.52	115.82
	600	69.274	39.037	2440.50	2.91	0.56	176.11
	700	70.335	38.6955	2275.10	2.95	0.55	166.69

As the calcination temperature rises, the coercivity values (*Hc*) grow as well. According to Raghvendra et al.[29], The rise in coercive values is related to the increase in the effective anisotropy area. The A-sublattice has a lower magnetization than the B-sublattice due to differences in the ion-electron exchange interaction in the overall magnetization[27]. The observed increase in the magnetic moment can be attributed to the elevation of calcining temperature, which results in the repositioning of the dominant Fe^{3+} ions at B-sites. One possible explanation for this phenomenon is that Fe^{3+} ions exhibit a higher magnetic moment compared to Co^{2+} ions[30]. The determination of the magnetic hardness of a material is contingent upon the squareness ratio (S), which is indicative of the anisotropy inherent in the system. S. I. Ahmad et al.[31] have reported that exchange-coupled interaction remains present for values of (S) greater than 0.5, while magneto-static interactions occur when (S) is less than or equal to 0.5. The results indicate that the values of (S) tend towards being greater than 0.5. The exchange between nanoparticles leads to their interaction.

3.2 CoFe2O4/SiO2 nanocomposites

3.2.1 XRD studies

Fig 6 depicts the XRD patterns of nanocomposites $CoFe_2O_4/SiO_2$ prepared by the standard ceramic process, in which SiO_2 with varying percentages (0, 20, 40, and 60%) was mixed with $CoFe_2O_4$ nanoparticles calcined at 700℃. There are no indications of impurities, as all index peaks correspond to cubic spinel. The X-ray diffraction (XRD) pattern displays reflection peaks that are indicative of the crystal structures of cobalt ferrites. Specifically, the peaks correspond to the (111), (220), (311), (222), (400), (422), (511), and (440) planes. The X-ray diffraction (XRD) patterns exhibit peak positions that correspond precisely to the typical pattern observed for pure $CoFe_2O_4$, as documented in reference card number ICSD 00-001-1121. The X-ray diffraction (XRD) patterns of the composite indicate the lack of the silica phase, implying its presence in an amorphous state[32].

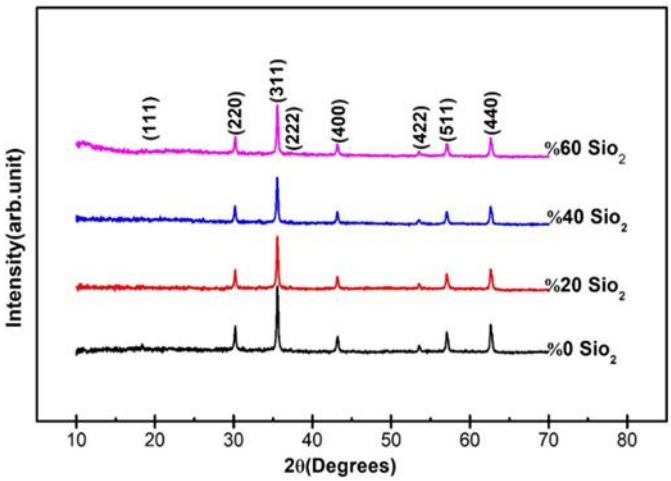

Figure 6: XRD patterns of $CoFe_2O_4/SiO_2$ nanocomposites with different ratios (0, 20, 40, and 60%).

Table 5: The Structural parameters of $CoFe_2O_4/SiO_2$ nanocomposites with different ratios (0, 20, 40, and 60%).

Composition	*Mixing ratio%*	2 Theta	*FWHM*	*D* (nm)	*a*(Å)	ρ_x(g/cm^3)	L_A(Å)	L_B(Å)
$CoFe_2O_4/SiO_2$	0	35.653	0.162	46.50	8.3454	5.362	3.614	2.951
	20	35.513	0.19	43.89	8.3771	5.301	3.627	2.962
	40	35.507	0.18	46.32	8.3785	5.298	3.628	2.962
	60	35.511	0.17	49.05	8.3777	5.300	3.628	2.962

As SiO_2 mixing increases in cobalt ferrite nanoparticles, the change in crystalline size (D) remains unstable, indicating that SiO_2 mixing affects grain growth while sustaining spinel phase formation. The variation in crystalline size can be associated with the disparity between the driving force for grain boundary motion and the retarding force exerted by SiO_2[33]. The increase in silica ratio at 20% lead to an increase in the hopping length at both A and B sites, while there are no discernible changes in the hopping length as silica increases from 40% to 60%. There is the possibility that the enhanced hopping length is due to the redistribution of cations between the tetrahedral (A- sites) and octahedral (B- sites).[34]. X-Ray Density (ρ_x) of $CoFe_2O_4/SiO_2$ samples decreases as silica value increases, it change from 5.362 to 5.300, as shown in table 5. The noticed behavior can be attributed to a decrease in molecular weight. The reason for this can be attributed to the fact that silica possesses a lower atomic weight in comparison to cobalt[20].

3.2.2 FT-IR analysis of CoFe2O4/SiO2 nanocomposites

The FT-IR spectra of $CoFe_2O_4/SiO_2$ nanocomposites that were palletized with KBr are presented in Figure 7. The spectral range analyzed was 400-4000 cm^{-1}. The absorption bands at v_1 and v_2 in all the nanocomposites samples are attributable to the intrinsic lattice vibration of the chemical bond (O-$M_{Oct.}$-O) at the octahedral (B site) and the chemical bond (O-$M_{tet.}$-O) at the tetrahedron (A site)[22].

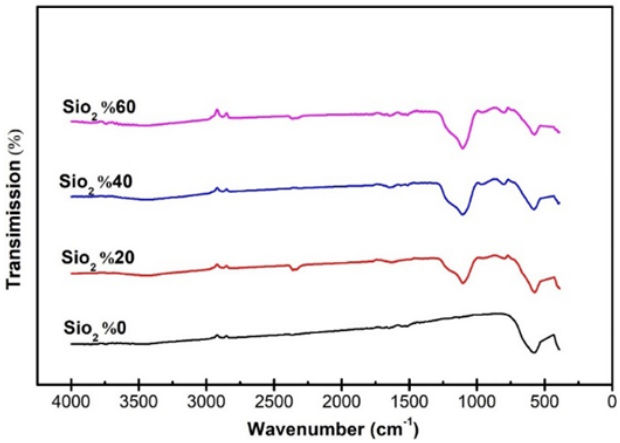

Figure 7: FTIR patterns of $CoFe_2O_4/SiO_2$ nanocomposites with different ratios (0, 20, 40, and 60%).

The spectral features observed indicate the formation of a spinel ferrite arrangement. The absorption bands observed for $CoFe_2O_4/SiO_2$ at (0, 20, 40, and 60%) within the ranges of 374.19, 463.81, 574.79, 811.02, and 1104.2 cm^{-1} (as presented in Table 6) are indicative of the symmetric and asymmetric expansion vibrations of Si-O-Si. These results suggest the formation of amorphous SiO_2[35]. Fig. 7 shows that when SiO_2 nanoparticles are mixed, the absorption bands (v_1) and (v_2) shift towards lower frequencies compared with that in pure $CoFe_2O_4$. The observed phenomenon can be attributed to the $CoFe_2O_4$ modified with SiO_2[36].

Table 6: The wave number of FT-IR spectroscopy of $CoFe_2O_4/SiO_2$ nanocomposites with different ratios (0, 20, 40, and 60%).

Composition	*Mixing ratio%*	*FTIR frequency bands (cm^{-1})*				
		v_1	v_2	v_3	v_4	v_5
$CoFe_2O_4/SiO_2$	0	574.79	374.19	--------	--------	--------
	20	572.67	372.87	1104.2	811.02	463.81
	40	572.03	372.84	1104.2	811.02	463.81
	60	570.77	370.05	1104.2	811.02	463.81

3.2.3 FE-SEM study of CoFe2O4/SiO2 nanocomposites.

The surface morphology and particle size of $CoFe_2O_4/SiO_2$ nanocomposites calcined at 700 °C were examined using FE-SEM images. The image displayed in Figure 8 (a) showcases $CoFe_2O_4$ in its unadulterated form, devoid of any SiO_2. Spherical crystallites with the majority of crystals aligned in the same direction can be formed by fashioning a dense structure visible from the shape. All particles seem to be roughly the same size 46.50 nm). Fig. 8 (b) displays a homogenous microstructure with evenly distributed smaller particles. Fig. 8 (c) demonstrates bigger particles than Figure 8 (b). Figure 8 (d) had a different morphology from the previous image, with agglomerated particles of varying sizes and shapes. Figures 8(b-d), from which we can deduce that the silica network contains nanoparticles of $CoFe_2O_4$ that are well-crystallized, uniformly scattered, and almost spherical. Furthermore, the surface structure of NPs is relatively uneven, consisting of smaller subunits. In the FE-SEM image, some aggregates can be observed and this may mostly be due to the interaction that occurs naturally between magnetic nanoparticles.

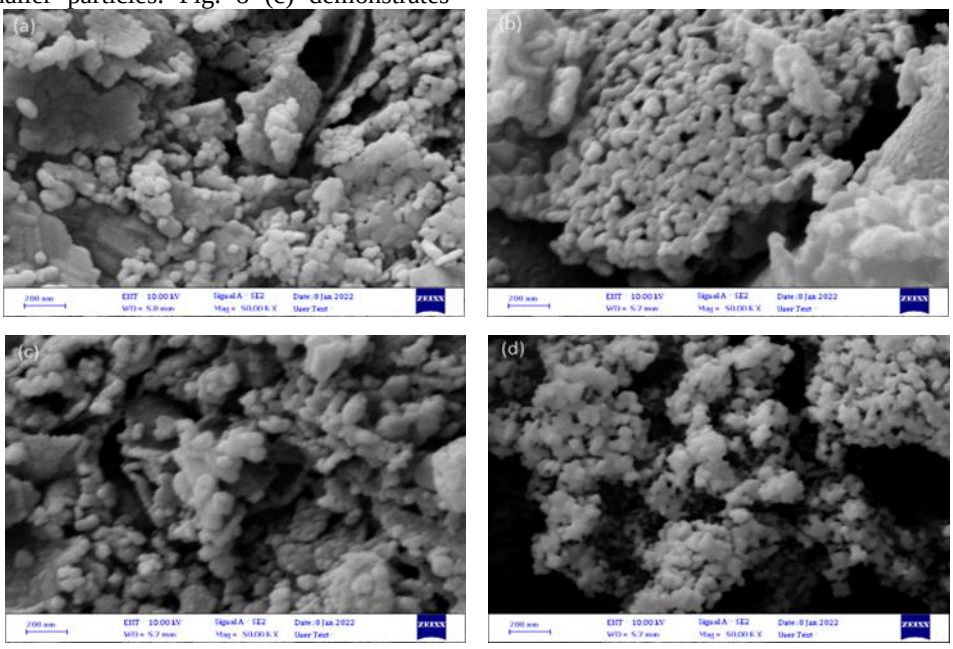

Figure 8: FE-SEM images of $CoFe_2O_4/SiO_2$ nanocomposites with different ratios of silica (a) 0 %, (b)20 %, (c) 40 %, and (d) 60% %.

Table 7: Average crystallite size and particle size of $CoFe_2O_4/SiO_2$ nanocomposites determined from XRD and FE-SEM for the different ratios of silica (0, 20, 40, and 60%).

Composition	*Mixing ratio%*	*D(nm)* XRD	*D(nm)* FE-SEM
$CoFe_2O_4/SiO_2$	0	46.50	51.97
	20	43.89	46.74
	40	46.32	50.99
	60	49.05	54.22

As shown in Figure 9, an energy dispersive spectroscopy (EDS) technique was utilized to determine the elemental compositions of nanoparticles. This technique was activated by an electron beam with a 10 keV energy as illustrated in Fig. 9(a-d). The EDS analysis indicates that the created nanocomposite contains significant amounts of the elements Cobalt, iron, Oxygen, and Silica. The apparent height of the peak of silicon increases in tandem with the increasing Si mixing concentration. The EDS analysis indicated the following weight ratios for the elements Co, Fe, O, and Si, as depicted in insets figure 9(a-d).

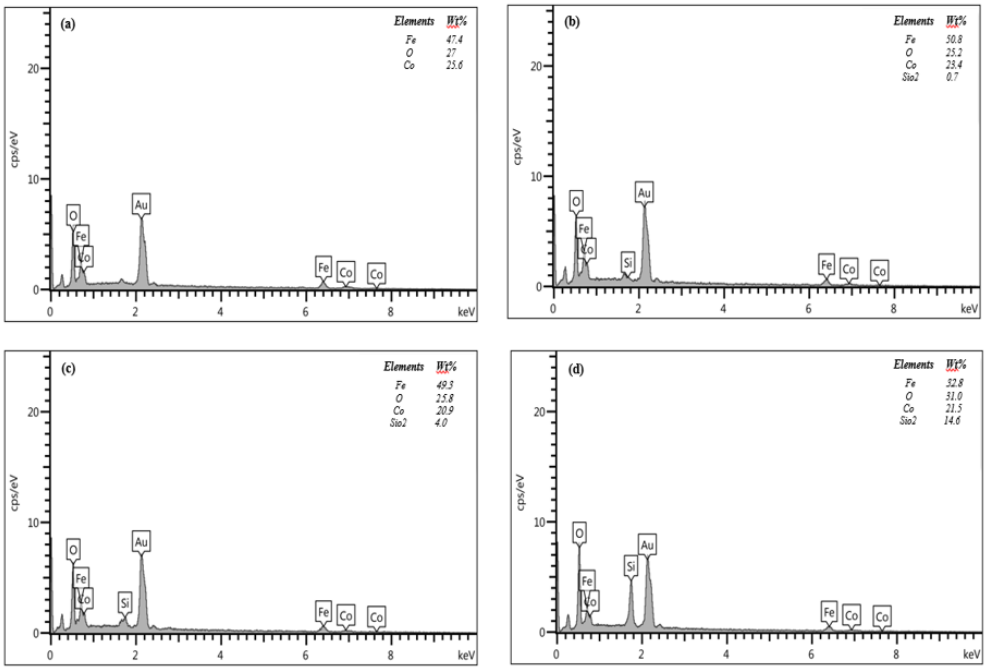

Figure 9: EDS spectra of $CoFe_2O_4/SiO_2$ nanocomposites with different ratios of silica (a) 0 %, (b)20 %, (c) 40 %, and (d) 60% %.

3.2.4 Magnetic measurement of CoFe2O4/Sio2 nanocomposites.

The M-H loops of $CoFe_2O_4/SiO_2$ nanocomposites with varying percentages of SiO_2 (0, 20, 40, and 60%) are illustrated in Fig. 10, and their magnetic property values are listed in Table (8). The saturation magnetization (*Ms*) and magnetic moment (n_B) of the nanocomposite samples decrease significantly as the SiO_2 mixing ratio increases. At 0% silica, the saturation magnetization and magnetic moment (n_B) of $CoFe_2O_4/SiO_2$ nanoparticles were the highest at 70. 335 emu.g^{-1} and 2.95 μ_B, respectively. At 60% silica, the saturation magnetization and magnetic moment were the lowest at 41.403 emu.g^{-1} and 1.74 μ_B, respectively. Interatomic spacing, Vacancies, and low coordination numbers may explain the drop in (*Mr*) with increased SiO_2 mixing[17], whereas the reduction in the magnetic moment is associated with an elevation in SiO_2 occupancy at (B-sites)[19].

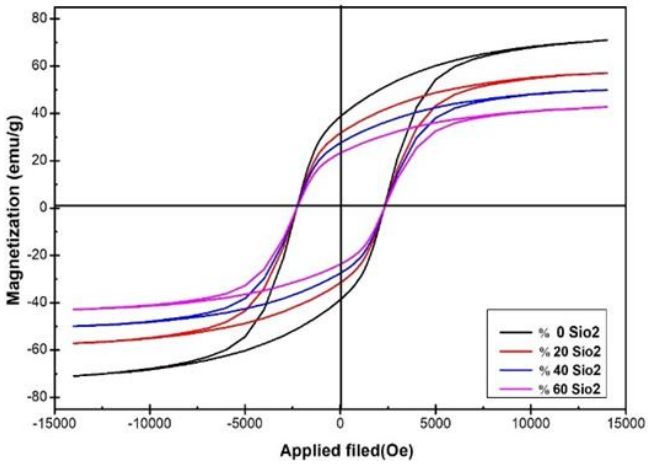

Figure 10: Hysteresis curves of $CoFe_2O_4/SiO_2$ nanocomposites with different ratios of silica (0, 20, 40, and 60%).

The remnant magnetization (*Mr*) of $CoFe_2O_4/SiO_2$ nanocomposites decreases with increasing SiO_2 content, from (38.695 emu.g^{-1}) at 0% SiO_2 to (23. 299 emu.g^{-1}) at 60%, and has similar behavior for the saturation magnetization. The development of non-crystalline SiO_2 on the surface of ferrite nanoparticles may be explained by such a decrease[37].

Table 8: Magnetic properties of $CoFe_2O_4/SiO_2$ composites for different silica ratios (0, 20, 40, and 60%).

Composition	*Mixing ratio %*	*Ms* (emu.g^{-1})	*Mr* (emu.g $^{-1}$)	*Hc*(Oe)	n_B (μ_B)	*Mr/ Ms*	$K \times 10^3$ (emu. Oeg^{-1})
$CoFe_2O_4/SiO_2$	0	70.335	38.695	2414.10	2.95	0.55	176.87
	20	56.321	31.791	2265.00	2.36	0.56	132.88
	40	49.215	27.494	2300.00	2.07	0.56	117.91
	60	41.403	23.299	2585.60	1.74	0.56	111.51

The coercive force values (*Hc*) fall from 2414.10 Oe ($CoFe_2O_4$) to 2265.00 Oe as the mixing content SiO_2 increases at rate of 20%. However, the coercive force values increase from 2300.00 Oe (40%) to 2585.60 Oe (60%) with an increase in the mixing ratio of SiO_2. The seen reduction in coercivity with an increase in SiO_2 mixing can be assigned to a corresponding reduction in the anisotropy field, thereby resulting in a reduction of the motion for the domain walls[38]. The rise in $CoFe_2O_4/SiO_2$ coercivity (at 40% to 60%) may be due to an increase in magnetic crystalline anisotropy (*K*)[17].

The degree of squareness influences whether or not there is grain exchange. Since (*Mr* /*Ms*) values are higher than 0.5, the results indicate an exchange-coupled interaction[17] exists between the nanoparticles. The magnetic anisotropy (*K*) values fall from 176.87 to 111.51×10^3 emu.Oeg^{-1} as the SiO_2 mixing ratio increases. The presence of Co^{2+} ions on the octahedral (B-sites) is the primary cause of the high magnetic anisotropy of $CoFe_2O_4$, and this fact may be explained in terms of the effect of SiO_2 mixing on the cation site occupancies. Therefore, *K* is decreased if SiO_2 enters the octahedral (B-site) and at least some Co^{2+} ions are displaced from the octahedral (B-site) to the tetrahedral (A-site)[39].

3.2.5 Dielectric measurements

The investigation of the dielectric properties of ferrite nanoparticles concerning their behavior under an applied AC electric field offers valuable knowledge regarding the mechanism of electrical conduction. The present term is influenced by various factors such as production technique, stoichiometric ratio, ionic charge, porosity, grain dimensions, and cation allocation within tetrahedral and octahedral structures[40]. Fig. 11(a-d) illustrates the dielectric parameters of synthesized $CoFe_2O_4/SiO_2$ nanocomposites with different ratios of silica (0, 20, 40, and 60 %).

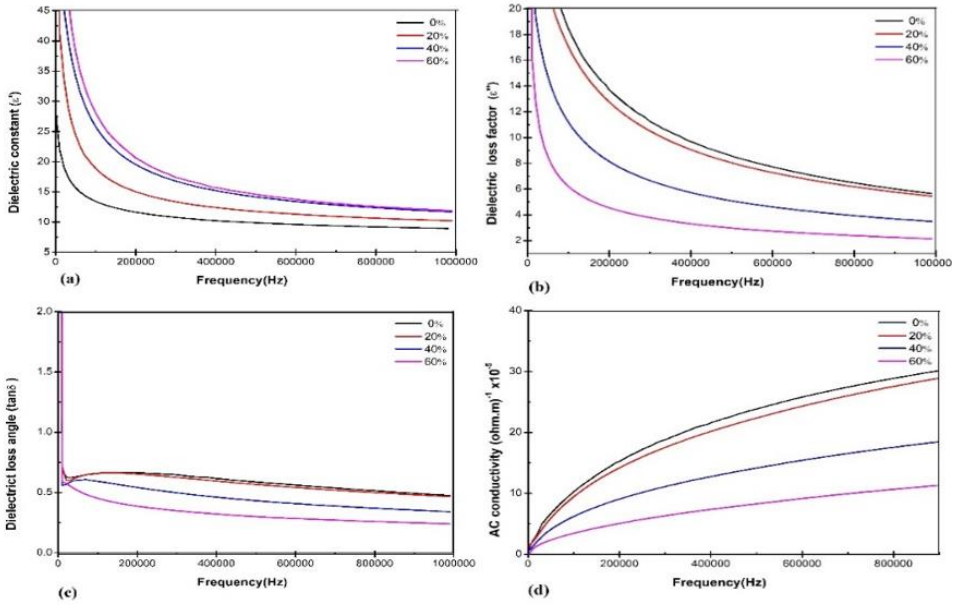

Figure 11: Dielectric properties of $CoFe_2O_4/SiO_2$ nanocomposites with different ratios of silica (0, 20, 40, and 60 %) as a function of frequency, (a) dielectric constant(ε'), (b) dielectric loss factor (ε''), (c) dielectric loss angle (tan δ), and (d) AC conductivity (σ_{ac}).

Using the following equations[20], the dielectric characteristics of synthesized ferrite nanocomposites were determined.

$$\varepsilon' = \frac{Cd}{\varepsilon_o A} \quad (9)$$

$$\varepsilon'' = \varepsilon' \tan\delta \quad (10)$$

$$\sigma_{ac} = 2\pi f \varepsilon_o \varepsilon' \tan\delta \quad (11)$$

where *C* is the pellet's capacitance measured in farads and *d* is the pellet's thickness measured in meters, and *A* is the cross-sectional area, ε_o is the free space permittivity constant, and f is the frequency.

Figure 11 (a) presents an illustration of the electrical behavior exhibited by ferrites nanocomposite, At low frequencies, the dielectric constant demonstrates a significant increase in value, followed by a decrease as the frequency increases and eventually attains its minimum value at high frequencies[26]. Table 3 displays the determination of the dielectric constant (ε') at different frequencies. (200 kHz, 400 kHz, 600 kH, 800 and 1000KHz). Lower frequency measurements show a greater dielectric constant, which can be attributed to the coexistence of multiple polarization mechanisms, such as space charge, dipolar, ionic, and electronic polarization. These mechanisms are known to diminish as the frequency increases. The observed raise in dielectric constant at lower frequencies may be related to the coexistence of various polarization mechanisms, such as space charge, dipolar, ionic, and electronic, which exhibit a diminishing effect as the frequency is raised[25]. At elevated frequencies, it has been observed that any element that contributes to polarization demonstrates a reaction slowly to an external field. This leads to a decrease in the dielectric constant, which can be attributed exclusively to the effect of electric polarizability[17]. As shown in Figure 11(a), when the amount of SiO_2 is raised to 60%, the dielectric constant (ε') also rises, a result that is in great agreement

with earlier reports by Q.M. Ahkam et al. and A.B. Kadam et al.[14, 41]. The incident frequency, which affects the dielectric constant, may be controlled via space charge polarizations. When an electric field is applied, a process known as charge entrapment takes place, which leads to the buildup of space charge at the boundaries of the grains, consequently, this results in an elevation of the dielectric constant. Dielectric loss pertains to the dissipation of electromagnetic energy within a dielectric substance and can be characterized by the dielectric loss angle (represented by the symbol $tan\ \delta$) and the dielectric loss factor (denoted by ε'')[42]. Fig. 11(b and c) depicts the dielectric loss angle and dielectric loss factor of $CoFe_2O_4/SiO_2$ as a function of frequency. Both showed a decreasing trend as the frequency increased and then stayed constant at high values, which is a characteristic of any ferrite material. Koop's idea[43] explains the frequency-dependent reduction in the values of each ($tan\ \delta$) and (ε''). Within the high range of frequency, characterized by low resistivity resulting from the grains, a minimal amount of energy suffices for electron hopping between two Iron oxides (Fe^{2+} and Fe^{3+}) situated at the octahedral (B-site). Conversely, in the low-frequency region, the grain boundary becomes active due to high resistivity, necessitating a substantial amount of energy for electron hopping between two Fe ions located at the (B-site)[43].

Dielectric loss has large values for pure cobalt ferrite, however, these values decrease with increasing SiO_2 content (0-60%) in $CoFe_2O_4$ nanocomposite. The preparation method, Fe^{2+} concentration, density, and structural homogeneity all affect the dielectric loss angle and factor. These properties make them appropriate for high-frequency applications[41].

Table 9: Dielectric properties of $CoFe_2O_4/SiO_2$ nanocomposites with different ratios of silica (0, 20, 40, and 60 %) as a function of various frequency.

Frequency (kHz)	*Dielectric parameters*	0% SiO_2	20% SiO_2	40% SiO_2	60% SiO_2
200	ε'	12	14.5	17.03	18.8
	ε''	14.1	12.5	7.8	4.5
	tan δ	0.63	0.61	0.57	0.37
	σ_{ac}	15.1	14.1	8.8	5.1
400	ε'	10.1	12.5	15.3	16
	ε''	10	9	5.8	3.8
	tan δ	0.60	0.59	0.5	0.33
	σ_{ac}	22.6	20.02	12.5	7.4
600	ε'	9	11.3	13.2	13.3
	ε''	8	7.5	4.3	2.8
	tan δ	0.58	0.57	0.42	3.02
	σ_{ac}	25.7	24.0	15	9.1
800	ε'	8.5	11	13	13.01
	ε''	6.3	6.1	3.9	2.4
	tan δ	0.54	0.53	0.32	2.76
	σ_{ac}	27.4	25.3	16.2	11.5
1000	ε'	8	9	11.3	11.4
	ε''	5.7	5.9	3.8	2.2
	tan δ	0.5	0.49	0.25	0.22
	σ_{ac}	30	27.03	17.1	12.3

Cobalt-doped SiO_2 was observed to have a similar ac conductivity (σ_{ac}) pattern by Q. M. Ahkam et al.[14]. Conductivity rises with frequency, as shown in Fig. 11(d), which plots conductivity against frequency. The transition of Fe^{3+} ions from the tetrahedral site to the octahedral site is difficult and inefficient, which causes a decline in the couple's number made up of ions with the charges of Fe^{2+} and Fe^{3+}. As a direct consequence of this, the amount of hopping that occurs between ferrites' electrons during the conduction process is reduced. The conductivity values of pure ($CoFe_2O_4$) and 60% of SiO_2 mixed ($CoFe_2O_4$) were found to be the greatest and lowest, respectively. it was discovered in the current investigation that increasing the SiO_2 mixing decreases ac conductivity (σ_{ac}), which contradicts a previous work by K. Nadeem et al.[17].

Conclusions

Using the sol-gel auto-combustion method, $CoFe_2O_4/SiO_2$ ferrite nanocomposites (SiO_2=0, 20, 40, and 60%) were effectively synthesized. Each sample exhibited the behavior typical of cubic spinel ferrite nanocomposites, as confirmed by XRD and FT-IR. Dependent on the calcination temperature, crystallite size changes from (33.46-46.50 nm), X-ray density from (5.312-5.362 g/cm^3), and hopping length from (3.625-3.614 Å). Depending on the SiO_2 mixing ratio, crystallite size changes from (46.50-49.05 nm), x-ray density (5.301-5.300 g/cm^3), and hopping length from (3.627-3.628 Å). FE-SEM images demonstrated that particle size grows during calcination. and mixing SiO_2 ratio increases. Co, Fe, SiO_2, and O were found in all ferrites using EDS. Vibrating Sample Magnetometer measurements show that all pure and mixing samples displayed ferrimagnetic behavior at various calcination temperatures and SiO_2 mixing ratios. Additionally

stated that at 700 °C, pure and doped samples' maximum saturation magnetization (*Ms*) values were 70.335 emu.g^{-1} and 70.335 emu.g^{-1}, respectively. Dielectric factors like (ε', ε'', and $tan\delta$) decreased as frequency rose due to electron hopping between ferrous (Fe^{2+}) and ferric (Fe^{3+}) ions. At high frequencies, they became constant. The conductivity (σ_{ac}) was noticed to grow with frequency. Depending on the SiO_2 mixing ratio, $CoFe_2O_4/SiO_2$ at 200(kHz), the dielectric constant (ε') changes from 12-18.8 with mixing 60% to pure substance. However, the other parameters (ε″) change from (14.1-4.5), *tan δ* change from (0.63-0.37), and (σ_{ac}) change from (15.1-5.1 ohm.m^{-1}×10^{-5}), which decreases with increasing the maxing ratio from pure to 60%.

Conflict of interests

The authors declare that they have no known competing financial interests or personal relationships that could have appeared to influence the work reported in this paper.

Funding Information

This research was done by me only without the contribution of any author and on my funding.

Author contribution

The implementation and organizing of the research, the results analysis, and the writing of the publication were all equally shared among the authors.

Funding

No financial support was provided for the research, writing, or publication of this article.

References

1. D. M. Cruz, E. Mostafavi, A. Vernet-Crua, H. Barabadi, V. Shah, J. L. Cholula-Díaz, G. Guisbiers, and T. J. Webster, "Green nanotechnology-based zinc oxide (ZnO) nanomaterials for biomedical applications: a review," *Journal of Physics: Materials*, vol. 3, no. 3, pp. 034005, 2020.
2. V. Kalpana, and V. Devi Rajeswari, "A review on green synthesis, biomedical applications, and toxicity studies of ZnO NPs," *Bioinorganic chemistry and applications*, vol. 2018, 2018.
3. A. Jaramillo, R. Baez-Cruz, L. Montoya, C. Medinam, E. Pérez-Tijerina, F. Salazar, D. Rojas, and M. Melendrez, "Estimation of the surface interaction mechanism of ZnO nanoparticles modified with organosilane groups by Raman Spectroscopy," *Ceramics International*, vol. 43, no. 15, pp. 11838-11847, 2017.
4. W. Ahmad, and D. Kalra, "Green synthesis, characterization and anti microbial activities of ZnO nanoparticles using Euphorbia hirta leaf extract," *Journal of King Saud University-Science*, vol. 32, no. 4, pp. 2358-2364, 2020.
5. S. Singh, S. Munjal, and N. Khare, "Strain/defect induced enhanced coercivity in single domain $CoFe_2O_4$ nanoparticles," *Journal of Magnetism and Magnetic Materials*, vol. 386, pp. 69-73, 2015.
6. A. Goldman, *Modern ferrite technology*: Springer Science & Business Media, 2006.
7. M. S. Caetano, T. C. Ramalho, D. F. Botrel, E. F. da Cunha, and W. C. de Mello, "Understanding the inactivation process of organophosphorus herbicides: A DFT study of glyphosate metallic complexes with Zn^{2+}, Ca^{2+}, Mg^{2+}, Cu^{2+}, Co^{3+}, Fe^{3+}, Cr^{3+}, and Al^{3+}," *International Journal of Quantum Chemistry*, vol. 112, no. 15, pp. 2752-2762, 2012.
8. S. Nodo, T. Yamamoto, T. Yanase, T. Shimada, and T. Nagahama, "Characterization of magnetic properties of ultrathin $CoFe_2O_4$ films by utilizing magnetic proximity effect," *Solid State Communications*, vol. 306, pp. 113762, 2020.
9. Z. Zi, Y. Sun, X. Zhu, Z. Yang, J. Dai, and W. Song, "Synthesis and magnetic properties of $CoFe_2O_4$ ferrite nanoparticles," *Journal of Magnetism and Magnetic Materials*, vol. 321, no. 9, pp. 1251-1255, 2009.
10. D. S. Mathew, and R.-S. Juang, "An overview of the structure and magnetism of spinel ferrite nanoparticles and their synthesis in microemulsions," *Chemical engineering journal*, vol. 129, no. 1-3, pp. 51-65, 2007.
11. S. M. Montemayor, L. Garcia-Cerda, J. Torres-Lubian, and O. Rodriguez-Fernandez, "Comparative study of the synthesis of $CoFe_2O_4$ and $NiFe_2O_4$ in silica through the polymerized complex route of the sol–gel method," *Journal of sol-gel science and technology*, vol. 42, pp. 181-186, 2007.
12. Y. Köseoğlu, F. Alan, M. Tan, R. Yilgin, and M. Öztürk, "Low temperature hydrothermal synthesis and characterization of Mn doped cobalt ferrite nanoparticles," *Ceramics International*, vol. 38, no. 5, pp. 3625-3634, 2012.
13. T. P. Yadav, R. M. Yadav, and D. P. Singh, "Mechanical milling: a top down approach for the synthesis of nanomaterials and nanocomposites," *Nanoscience and Nanotechnology*, vol. 2, no. 3, pp. 22-48, 2012.
14. Q. M. Ahkam, E. U. Khan, J. Iqbal, A. Murtaza, and M. T. Khan, "Synthesis and characterization of cobalt-doped SiO_2 nanoparticles," *Physica B: Condensed Matter*, vol. 572, pp. 161-167, 2019.
15. S. Rostamzadehmansour, M. Seyedsadjadi, and K. Mehrani, "An investigation on synthesis and magnetic properties of manganese doped cobalt ferrite silica core-shell nanoparticles for possible biological application," *Int. J. Bio-Inorg. Hybd. Nanomat*, vol. 2, no. 1, pp. 271-280, 2013.
16. C. C. Chen, Y. P. Fu, and S. H. Hu, "Characterizations of TiO_2/SiO_2/Ni–Cu–Zn ferrite composite for magnetic photocatalysts," *Journal of the American Ceramic Society*, vol. 98, no. 9, pp. 2803-2811, 2015.
17. K. Nadeem, F. Zeb, M. A. Abid, M. Mumtaz, and M. A. ur Rehman, "Effect of amorphous silica matrix on structural, magnetic, and dielectric properties of cobalt ferrite/silica nanocomposites," *Journal of non-crystalline solids*, vol. 400, pp. 45-50, 2014.
18. M. Goodarz Naseri, E. B. Saion, H. Abbastabar Ahangar, A. H. Shaari, and M. Hashim, "Simple synthesis and characterization of cobalt ferrite nanoparticles by a thermal treatment method," *Journal of Nanomaterials*, vol. 2010, 2010.
19. A. Mohammad, S. Aliridha, and T. Mubarak, "STRUCTURAL AND MAGNETIC PROPERTIES OF Mg-Co FERRITE NANOPARTICLES," *Digest Journal of Nanomaterials & Biostructures (DJNB)*, vol. 13, no. 3, 2018.
20. A. M. Mohammad, S. M. A. Ridha, and T. H. Mubarak, "Dielectric properties of Cr-substituted cobalt ferrite nanoparticles synthesis by citrate-gel auto combustion method," *Int. J. Appl. Eng. Res*, vol. 13, no. 8, pp. 6026-6035, 2018.
21. J. Bezerra, R. Matos, B. Zucolotto, P. Pedra, and N. Ferreira, "Effects of different complexing agents on the physical properties of ZnO nanoparticles," *Materials Science and Technology*, vol. 35, no. 2, pp. 231-239, 2019.
22. R. S. Yadav, J. Havlica, J. Masilko, L. Kalina, J. Wasserbauer, M. Hajdúchová, V. Enev, I. Kuřitka, and Z. Kožáková, "Impact of Nd^{3+} in $CoFe_2O_4$ spinel ferrite nanoparticles on cation distribution, structural and magnetic properties," *Journal of Magnetism and Magnetic materials*, vol. 399, pp. 109-117, 2016.
23. I. Gul, W. Ahmed, and A. Maqsood, "Electrical and magnetic characterization of nanocrystalline Ni–Zn ferrite synthesis by co-precipitation route," *Journal of Magnetism and Magnetic Materials*, vol. 320, no. 3-4, pp. 270-275, 2008.
24. L. Kumar, P. Kumar, A. Narayan, and M. Kar, "Rietveld analysis of XRD patterns of different sizes of nanocrystalline cobalt ferrite," *International Nano Letters*, vol. 3, pp. 1-12, 2013.
25. S. Divya, P. Sivaprakash, S. Raja, S. E. Muthu, I. Kim, N. Renuka, S. Arumugam, and T. H. Oh, "Impact of Zn doping on the dielectric and magnetic properties of $CoFe_2O_4$ nanoparticles," *Ceramics International*, vol. 48, no. 22, pp. 33208-33218, 2022.

26. M. B. Jumaa, T. H. Mubarak, and A. M. Mohammad, "Synthesis and Characterization of Spinel Ferrite $Co_{0.8}Fe_{2.2}O_4$ Nanoparticle," *Synthesis,* vol. 15, no. 2, pp. 74-82, 2021.

27. A. Mohammad, M. Mohammed, and L. Hussein, "STRUCTURAL, MAGNETIC AND OPTICAL PROPERTIES OF $Co_{0.5}Ni_{0.5}Fe_2O_4$ NANOPARTICLES SYNTHESIZED BY SOL-GEL AUTO COMBUSTION METHOD," *Digest Journal of Nanomaterials and Biostructures,* vol. 15, no. 1, pp. 231-241, 2020.

28. R. Mohamed, M. Rashad, F. Haraz, and W. Sigmund, "Structure and magnetic properties of nanocrystalline cobalt ferrite powders synthesized using organic acid precursor method," *Journal of Magnetism and Magnetic Materials,* vol. 322, no. 14, pp. 2058-2064, 2010.

29. R. S. Yadav, J. Havlica, M. Hnatko, P. Šajgalík, C. Alexander, M. Palou, E. Bartoníčková, M. Boháč, F. Frajkorová, and J. Masilko, "Magnetic properties of $Co_{1-x}Zn_xFe_2O_4$ spinel ferrite nanoparticles synthesized by starch-assisted sol–gel autocombustion method and its ball milling," *Journal of Magnetism and Magnetic Materials,* vol. 378, pp. 190-199, 2015.

30. B. Purnama, and A. T. Wijayanta, "Effect of calcination temperature on structural and magnetic properties in cobalt ferrite nano particles," *Journal of King Saud University-Science,* vol. 31, no. 4, pp. 956-960, 2019.

31. S. I. Ahmad, A. Rauf, T. Mohammed, A. Bahafi, D. R. Kumar, and M. B. Suresh, "Dielectric, impedance, AC conductivity and low-temperature magnetic studies of Ce and Sm co-substituted nanocrystalline cobalt ferrite," *Journal of Magnetism and Magnetic Materials,* vol. 492, pp. 165666, 2019.

32. S. Zhang, D. Dong, Y. Sui, Z. Liu, H. Wang, Z. Qian, and W. Su, "Preparation of core shell particles consisting of cobalt ferrite and silica by sol–gel process," *Journal of alloys and compounds,* vol. 415, no. 1-2, pp. 257-260, 2006.

33. S. B. Khalifa, M. Gassoumi, A. B. Dhahbi, F. Alresheedi, A. Z. elAbdeen Mahmoud, and L. Beji, "The effect of the cobalt ferrites nanoparticles ($CoFe_2O_4$) on the porous silicon deposited by spin coating," *Alexandria Engineering Journal,* vol. 59, no. 3, pp. 1093-1098, 2020.

34. R. S. Yadav, I. Kuřitka, J. Vilcakova, P. Urbánek, M. Machovsky, M. Masař, and M. Holek, "Structural, magnetic, optical, dielectric, electrical and modulus spectroscopic characteristics of $ZnFe_2O_4$ spinel ferrite nanoparticles synthesized via honey-mediated sol-gel combustion method," *Journal of Physics and Chemistry of Solids,* vol. 110, pp. 87-99, 2017.

35. K. Nadeem, M. Shahid, and M. Mumtaz, "Competing crystallite size and zinc concentration in silica coated cobalt ferrite nanoparticles," *Progress in Natural Science: Materials International,* vol. 24, no. 3, pp. 199-204, 2014.

36. T. Ramesh, S. Bharadwaj, and S. R. Murthy, "Composites: preparation and magnetodielectric properties," *Journal of Materials,* vol. 2016, 2016.

37. L. Zhao, H. Yang, Y. Cui, X. Zhao, and S. Feng, "Study of preparation and magnetic properties of silica-coated cobalt ferrite nanocomposites," *Journal of materials science,* vol. 42, pp. 4110-4114, 2007.

38. K. Chandra, S. Singhal, and S. Goyal, "Magnetic and Mössbauer spectral studies of nano crystalline cobalt substituted magnesium ferrites ($Mg_x Co_{1-x}Fe_2O_4$)." pp. 247-252.

39. A. Franco Jr, F. e Silva, and V. S. Zapf, "High temperature magnetic properties of $Co_{1-x}Mg_xFe_2O_4$ nanoparticles prepared by forced hydrolysis method," *Journal of Applied Physics,* vol. 111, no. 7, pp. 07B530, 2012.

40. M. Vadivel, R. R. Babu, K. Sethuraman, K. Ramamurthi, and M. Arivanandhan, "Synthesis, structural, dielectric, magnetic and optical properties of Cr substituted $CoFe_2O_4$ nanoparticles by co-precipitation method," *Journal of magnetism and magnetic materials,* vol. 362, pp. 122-129, 2014.

41. A. Kadam, V. K. Mande, S. Kadam, R. Kadam, S. E. Shirsath, and R. B. Borade, "Influence of gadolinium (Gd^{3+}) ion substitution on structural, magnetic and electrical properties of cobalt ferrites," *Journal of Alloys and Compounds,* vol. 840, pp. 155669, 2020.

42. M. R. Siddiquah, "Effect of doping of various metal cations on structural, electrical and magnetic properties of nano cobalt ferrites," Quaid-i-Azam University Islamabad, Pakistan, 2008.

43. C. Koops, "On the dispersion of resistivity and dielectric constant of some semiconductors at audiofrequencies," *Physical review,* vol. 83, no. 1, pp. 121, 1951.